Journal of Materials Chemistry C

Surface ligation stage revealed through polarity-dependent fluorescence during perovskite nanocrystal growth

Journal:	*Journal of Materials Chemistry C*
Manuscript ID	TC-ART-11-2019-006545.R1
Article Type:	Paper
Date Submitted by the Author:	30-Mar-2020
Complete List of Authors:	Sadighian, James; University of Oregon, Department of Chemistry and Biochemistry Crawford, Michael; University of Oregon, Department of Chemistry and Biochemistry Suder, Tim; University of Oregon, Department of Chemistry and Biochemistry Wong, Cathy; University of Oregon, Department of Chemistry and Biochemistry

ARTICLE

Surface ligation stage revealed through polarity-dependent fluorescence during perovskite nanocrystal growth

Received 00th January 20xx,
Accepted 00th January 20xx

DOI: 10.1039/x0xx00000x

James C. Sadighian,[a] Michael L. Crawford [a], Timothy W. Suder, [a,b,c] and Cathy Y. Wong [a,d,e]

Methylammonium lead iodide perovskite ($MAPbI_3$) nanocrystals (NCs) exhibit favorable photophysics for a range of light emitting applications. A comprehensive mechanistic understanding of the nucleation and growth processes for these NCs is still elusive. Absorbance and fluorescence spectra were measured during a NC synthesis with kinetics limited by precursor solvation using a rapid sampling technique wherein syringe filters quench NC growth. The signal from well-capped NCs in the reaction mixture was isolated by the use of polar syringe filters, enabling spectroscopic observation of the surface ligation process. Our results indicate that the formation of these NCs involves a single stage of nucleation and growth, followed by a terminal surface ligation stage.

Introduction

Organic-inorganic hybrid perovskites are promising materials for a range of applications owing to their attractive electronic properties, such as low exciton binding energy, high carrier mobility, and low-cost synthesis. Solution processed, quantum-confined nanocrystals (NCs) of these materials are generating particular interest for light-emitting applications due to their exceptionally high fluorescence quantum yield coupled with a narrow and easily tunable emission spectrum in the visible wavelength region. This has driven significant research towards optimizing these NCs for applications in light-emitting devices, lasers, and optoelectronics[1–6] by changing precursors or adjusting initial reaction conditions to yield NCs with different electronic properties or morphologies.[7–14] A mechanistic understanding of nucleation and growth in these NCs would aid in this effort.

The classic model of NC formation proposed by LaMer comprises three discrete stages.[15–18] The precursor concentration must first increase until a critical supersaturation point has been reached. Self-nucleation then occurs until the precursor concentration has dropped below the critical nucleation concentration, at which point the newly-formed nuclei begin growing to form NCs. The duration of the self-nucleation stage is a key factor in determining the size distribution of the resulting NCs. Syntheses that follow a 'burst nucleation' mechanism aim to rapidly exceed the critical supersaturation point. Strategies include the rapid injection of a solution containing a high concentration of one of the precursors, rapidly lowering the temperature of the reaction, or adding a co-solvent in which the precursor is less soluble.[7,11,19–24]

Following nucleation, the rate of growth for some NCs can be described as a function of precursor diffusion,[17,18] but for other NCs the growth stage may be more complicated. Recent work suggests that the perovskite crystal structure is not fully formed at the beginning of this growth period, instead existing as a plumbate complex with cations (methylammonium, formamadinium, cesium, etc.) still diffusing into the lattice.[25–28] Additionally, Ostwald ripening, where smaller NCs are re-solubilized and consumed by more stable, larger NCs, can cause defocusing of the size distribution.[29–32]

The surface plays a significant role in the nucleation and growth of NCs.[33–37] Understanding the surface is key for understanding the electronic structure, function, and growth of NCs owing to their large surface-to-volume ratios. Surface ligands are commonly used to prevent aggregation and passivate electronic trap states that arise from dangling bonds at unoccupied surface sites.[37–39] These trap states occupy energy levels between the HOMO and LUMO bands and significantly reduce NC fluorescence quantum yield.

One possible model of NC surface evolution during formation is illustrated in Figure 1a, where the NCs after the nucleation event are well-passivated while they continue to grow. During this process, the decreasing quantum confinement causes a redshift in the fluorescence spectrum. Recently, a terminal stage of colloidal NC formation has been proposed after the NCs have completed their growth.[40] The redshift of the fluorescence spectrum and the increase in fluorescence intensity typically ascribed to the growth stage are

[a] Department of Chemistry and Biochemistry, University of Oregon, Eugene, Oregon, 97403, United States
[b] Department of Chemistry, West Virginia Wesleyan College, Buckhannon, West Virginia, 26201, United States
[c] Department of Physics, West Virginia Wesleyan College, Buckhannon, West Virginia, 26201, United States
[d] Oregon Center for Optical, Molecular, and Quantum Science, University of Oregon, Eugene, Oregon, 97403, United States
[e] Materials Science Institute, University of Oregon, Eugene, Oregon, 97403, United States

† Footnotes relating to the title and/or authors should appear here.
Electronic Supplementary Information (ESI) available: [details of any supplementary information available should be included here]. See DOI: 10.1039/x0xx00000x

instead shown to result from increased passivation of NCs by ligands attaching to dangling bonds on the NC surface, Figure 1b. Classical nucleation and growth can also be followed by a secondary nucleation event wherein small, poorly-capped NCs from the first growth stage aggregate, Figure 1c.[41] For NCs that exhibit aggregative nucleation and growth following classical nucleation and growth, it is the aggregative nucleation stage that determines the final nanocrystal size distribution. While these mechanisms have been observed and rigorously studied in chalcogenide NCs[42–48] and other systems,[49–53] additional measurements are required to determine which, if any, of these models can be used to accurately describe the surface during the formation of hybrid perovskite NCs.

Tracking NC absorbance and emission spectra is a quick, simple, and effective way to monitor NC growth and passivation.[54] The decrease in quantum confinement as the NC diameter increases causes a red shift in their band edge absorbance and fluorescence. Additionally, increased emission intensity indicates the passivation of surface trap states by capping ligands.[39,55,56,40] The most common method of sampling NCs during growth involves sequentially extracting aliquots of the reaction mixture and centrifuging each sample for several minutes to remove solid reactants, quenching the reaction and minimizing sources of scatter. The absorbance and fluorescence of these samples can then be measured.[8,14,19,25,28,57–59] However, during centrifugation individual NCs can continue to grow or dissolve back into precursors, and the fractional passivation of their surface by ligands can change. As a result, this sampling method fails to provide an accurate snapshot of the NCs and their surface during growth. In situ spectroscopic measurements of CdSe NCs have been conducted using a transmission-reflectance dip probe, removing the sampling problem.[60] This technique is most effective when measuring reaction mixtures without an excess of solid precursor so scatter at the tip of the probe is minimal. Fluorescence measurements during growth require that the reaction mixture be sequentially sampled, and for a typical fluorimeter configuration the sample must be diluted to prevent inner-filter effects. While this may not negatively affect NCs with a stronger lattice, such as CdSe NCs, dilution causes hybrid perovskite NCs to exfoliate into nanoplatelets, radically altering their electronic properties.[61] The soft lattice of hybrid perovskites also limits the utility of in situ transmission electron microscopy (TEM) measurements during NC growth, as even fully grown, stable perovskite films and NCs may be damaged by the electron beam during TEM.[62–64] In situ measurements of absorbance, fluorescence, and small-angle X-ray scattering (SAXS) using microfluidic reactors[65–67] also provide insight, but these measurements occur under conditions that do not represent those found in a typical wet-lab synthesis.

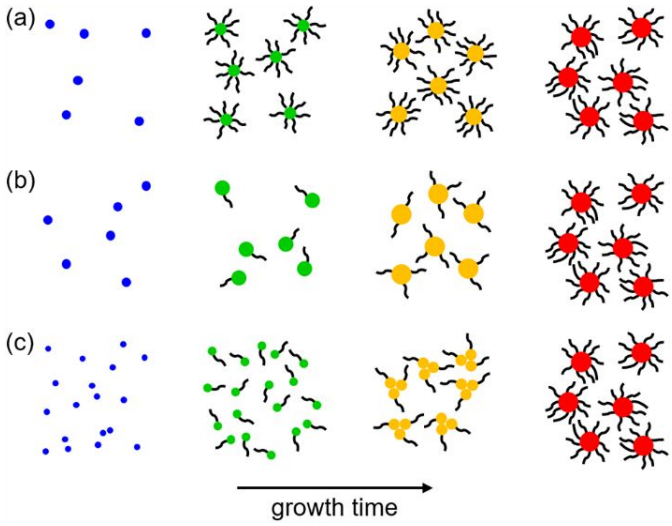

Figure 1: Models of the NC surface during growth. (a) The surfaces of nascent NCs are well-capped throughout growth. (b) Nascent NCs are poorly-capped during growth, only becoming well-capped in a distinct surface ligation stage near the end of NC formation. (c) Aggregative nanocrystal growth wherein smaller, poorly-capped NCs aggregate to form a larger NC.

Perovskite NCs are typically synthesized using either ligand-assisted reprecipitation (LARP)[7,19,59] or hot-injection[20] techniques, where nuclei are produced rapidly via burst nucleation[15,18,41,68] and subsequent NC growth can be complete in a matter of seconds to minutes. In these conventional synthetic methods, nucleation occurs in an environment that includes extreme temperature and/or concentration gradients, introducing sources of inhomogeneity to the nuclei and resulting NCs, limiting the scalability of the reaction. A non-polar solvent that reduces the solubility of the polar precursor salts can be used to increase homogeneity in the reaction mixture during nucleation and growth. Small amounts of organic ligand can then serve to mediate the synthesis by solvating the precursor, making it available for nucleation. This solvation step limits the rate of the reaction, allowing the reaction to be well-mixed during the formation process. This increases the homogeneity of the reaction environment, improves reaction scalability, and substantially increases the number of measurements that can be made during NC growth.[69]

In this paper, we measure absorbance and fluorescence of the reaction mixture during a ligand-mediated synthesis of methylammonium lead iodide ($MAPbI_3$) NCs. Since the lead iodide and methylammonium iodide precursors are insoluble in the non-polar solvent, aliquots of the reaction mixture contain suspended solids that can scatter light and interfere with spectroscopic measurement. Centrifugation can remove these solids, but the species in the sample may evolve during this procedure. To decrease the delay time between aliquot removal and measurement, we use syringe filters to quickly remove solid components from the reaction mixture. The absorbance and fluorescence of sequentially extracted aliquots of the reaction mixture show the evolution of the species within the mixture and their dynamic electronic structure. Additional insight into the physical and electronic structure of the nuclei and growing NCs is gained by comparing measurements of the reaction mixture after it passes through filters of different polarities. These experiments show that the formation of hybrid perovskite NCs includes a surface ligation stage that increases NC stability and photoluminescence.

Experimental

Absorbance and Fluorescence Measurements

$MAPbI_3$ NCs were synthesized via a solvation-mediated synthesis previously reported.[58,70] Two aliquots of the reaction mixture were extracted at 16 discrete time points during five separate syntheses. Each aliquot was filtered through either a PTFE or nylon membrane syringe filter into a 1 mm path length cuvette. This removed solid precursors that cause scatter, enabling nearly in situ absorbance and fluorescence measurements using a homebuilt instrument, Figure S1. Spectra measured for aliquots extracted at the same time points during the five separate syntheses were averaged, shown in Figure 2. The standard deviation in the spectra at four selected time points is indicated by the shaded region. The standard deviation for all time points is shown in Figure S3. Further information regarding the reagents, synthesis, and sampling may be found in the supplemental information.

Transmission Electron Microscopy

TEM images were obtained with an FEI Titan 80-300 kV STEM equipped with a C_s image corrector operating at 300 kV. The as-synthesized NCs were filtered and further diluted in hexane immediately before drop-casting onto lacey carbon TEM grids with an ultrathin carbon support film.

Results and Discussion

Transmission Electron Microscopy

Figure 2 shows TEM characterization of NCs grown for 120 minutes, equalling the longest reaction time used in any of our experiments. A high-angle annular dark-field scanning transmission electron microscopy (HAADF-STEM) image of NCs filtered through PTFE is shown in Figure 2a, whereas a bright-field image of NCs filtered through nylon is shown in Figure 2b. The two samples of NCs exhibit similar circularities of 92±.2 and 93±.03 for PTFE- and nylon-filtered NCs, respectively. This is in agreement with previous literature reports that this synthesis produces highly spherical nanoparticles.[58] Filter material is shown to have little effect on the size of particles in the filtrate, Figure 2c,d, as filtration through PTFE and nylon each result in NCs with an average size of 3.7 nm ± 1 nm.

While TEM is commonly used to characterize NCs, rinses with anti-solvent and centrifugation are typically required to remove superfluous organic ligand before imaging, particularly at the high magnifications necessary for accurate size quantification. Without these steps, images suffer from poor contrast and uneven background intensity as the ligands polymerize under the high energy beam and deposit onto the TEM grid. The perovskite NC solutions may change as a result of these preparatory procedures, yielding TEM images that may not accurately reflect the original population.[71] Further, it is known that TEM causes irreversible damage to perovskite thin films.[63,72,73] Since the surface plays a central role in degradation,[74,75] the large surface-to-volume ratio of perovskite NCs renders them highly susceptible to damage during TEM

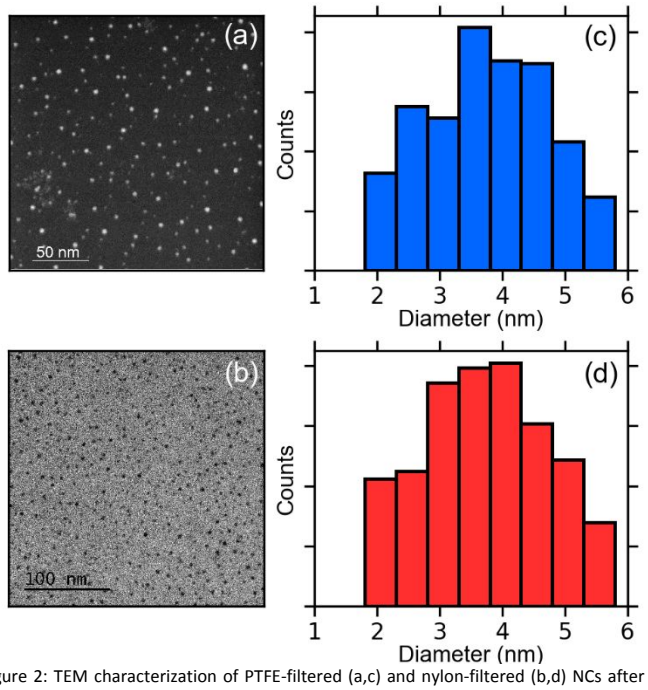

Figure 2: TEM characterization of PTFE-filtered (a,c) and nylon-filtered (b,d) NCs after 120 minutes of growth. Image of PTFE-filtered NCs was taken in HAADF-STEM (a), nylon-filtered NCs were imaged in bright-field TEM (b). Size distribution information shows both NC populations have an average size of 3.7 nm (n_{PTFE}=540, n_{nylon}=592).

measurements.[62–64] Consequently, unstable nascent NCs may degrade too quickly for reliable imaging and characterization. Rapid, non-destructive characterization techniques, such as optical spectroscopies, are necessary to study NCs sampled and filtered during early stages of nucleation and growth, when nascent, growing NCs are unstable.

Absorbance and Fluorescence Measurements

Aliquots filtered through the PTFE filters exhibit absorbance at 375 nm after 3 minutes, Figure 3. We attribute this to plumbate complexes that form at the beginning of $MAPbI_3$ syntheses.[27] The solution appeared to reach the critical nucleation threshold within the first 3 minutes, as indicated by the appearance of a broad fluorescence feature centered near 640 nm. The fluorescence intensity continued to grow over the first few minutes, alongside the onset of broad absorbance extending to 600 nm. After nine minutes of reaction time, two distinct peaks at 545 and 585 nm appeared in the absorbance spectrum and at 600 and 650 nm in the fluorescence spectrum. The fluorescence intensity continued to increase until 20 minutes of reaction time, at which point the 600 nm peak began to lose intensity and the spectrum started to redshift. This corresponded with the disappearance of the absorbance feature at 545 nm and a rapid increase in absorbance at 585 nm. The intensity of the 585 nm absorbance reached a maximum after 35 minutes of growth, then began to lose intensity while the band-edge absorbance shoulder at 635 nm exhibited significant growth. We attribute the absorbance at 635 nm to larger NCs that only weakly confine an exciton. Meanwhile, the fluorescence peak at 600 nm weakened substantially and the overall spectrum became significantly more unimodal. The spectrum continued to redshift and increase in intensity during

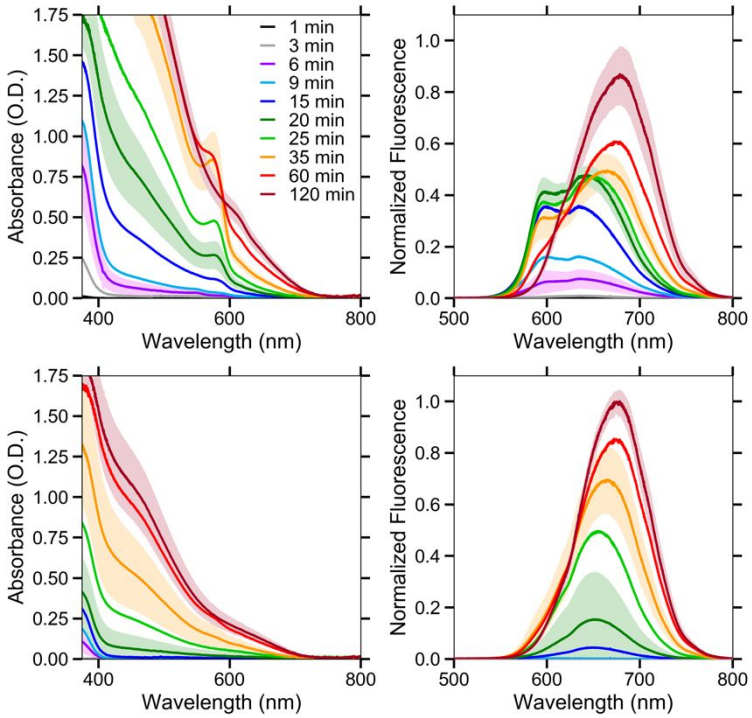

Figure 3: Absorbance (left) and fluorescence (right) of reaction mixture filtered through PTFE (top) or nylon (bottom). Traces represent an average of 5 syntheses with shaded areas showing standard deviations for selected time points

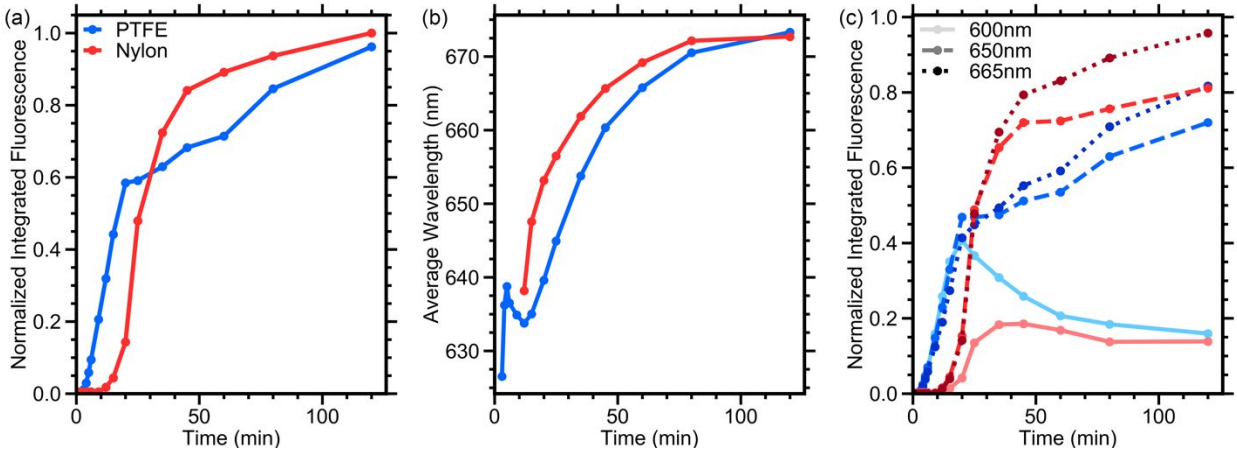

Figure 4: Comparison of fluorescence spectra for perovskite NCs during formation after filtering through PTFE (blue) or nylon (red). (a) Integrated fluorescence intensity. (b) Average emission wavelength. (c) Normalized fluorescence intensity at 600 nm (solid), 650 nm (dashed), and 665 nm (dotted).

the final hour of the synthesis. NC samples filtered through polar nylon membranes produced starkly different absorbance and fluorescence spectra, particularly during the beginning of NC formation. At early reaction times there was significantly less absorbance from plumbates, as these were more effectively removed by the polar nylon membrane. Emission was not detected until after 15 minutes of growth, when a weak and broad peak centered close to 650 nm was detected, characteristic of $MAPbI_3$ NCs that are only weakly confining the exciton, as opposed to the two peaks observed at 600 nm and 650 nm for NCs filtered through PTFE after an equivalent growth time. This suggests that the polar nylon filter removed the smaller NCs that would exhibit fluorescence at shorter wavelengths. Thus, we conclude that the smaller NCs must be poorly-capped by organic ligands. The exposed NC surface is polar and more likely to be adsorbed to the nylon filter. The intensity of the fluorescence spectrum grew rapidly and redshifted slightly between 15 and 35 minutes for the nylon-filtered samples. This corresponded to the beginning of the redshift observed in the fluorescence of PTFE-filtered NCs, although those spectra showed little change in overall intensity during the same time period. Following 35 minutes, the fluorescence of nylon-filtered NCs continued to gain intensity and redshift. The absorbance tail at 635 nm, which we ascribe to larger NCs, first appeared in nylon-filtered NCs after 20 minutes of growth and proceeded to slowly increase for the rest of the synthesis. Although this feature increased in intensity throughout the experiment, up to the last measurement at 120 minutes, the optical density was still much lower than in the NCs filtered through PTFE. However, despite the weaker absorbance, NCs filtered through nylon exhibit much stronger fluorescence with a narrower line shape than those filtered

through PTFE. This is further evidence that filtration by a nylon membrane removes poorly-capped NCs that contribute to absorbance but not fluorescence.

Plotting the integrated fluorescence at each time point revealed stark differences in the rate of intensity increase for NCs filtered through either PTFE or nylon, Figure 4a. PTFE-filtered NCs showed a sharp, linear increase in integrated fluorescence during the first 20 minutes of the reaction. Following 20 minutes there was a distinct change in the rate of intensity increase, though it remained linear. The change in integrated fluorescence intensity of nylon-filtered NCs during growth was sigmoidal, with an onset that was delayed until 15 minutes. The integrated fluorescence intensity of the nylon-filtered NCs increased rapidly and exceeded that of the NCs filtered through PTFE after 30 minutes. The rate of increase in fluorescence intensity slowed significantly after 50 minutes.

Figure 4b shows the average fluorescence wavelength at each time point during NC growth. Immediately after fluorescence was detected from the PTFE-filtered sample the spectrum began to redshift. As the 600 nm peak reached its maximum intensity after 20 minutes of growth, a slight blueshift in the average wavelength was observed as the intensity of the 600 nm peak overtook that of the lower energy 650 nm peak. This suggests that during this early stage of NC formation the population of small NCs that fluoresce at 600 nm grew faster than the population of larger NCs that fluoresce at 650 nm. Concurrently, the nylon-filtered sample began to exhibit detectable fluorescence after 15 minutes of growth that was redder than that of the PTFE-filtered sample. As the reaction proceeded until the final measurement at 120 minutes, the average emission wavelength for both samples approached 675 nm, typical for weakly-confined excitons in $MAPbI_3$ NCs.

Figure 4c shows the increase in fluorescence intensity during NC growth for the features at 600 nm, 650 nm, and 665 nm. The fluorescence of the PTFE-filtered samples at these three wavelengths increased initially at a similar rate. After 20 minutes of growth the fluorescence intensity at the three wavelengths began to diverge, providing insight into the source of the inflection point shown in 4a. The peak at 600 nm reached its maximum at 20 minutes before it started to decay, indicating that this species is being consumed by the formation of new, redder emissive nanoparticles. This could be due to aggregative growth or a coalescence/ripening process wherein particles dissolve and are consumed by larger particles that continue to grow. The fluorescence intensity measured at 650 nm most closely mimicked the integrated fluorescence intensity in the PTFE-filtered sample, Figure 4a, and continued to increase linearly, though at a slower rate than during the first 20 minutes of NC growth. The rate of increase in the fluorescence intensity at 665 nm slowed after 20 minutes of growth, but the intensity grew faster at 665 nm than at 650 nm, since the broad feature that spanned this wavelength range redshifted as its intensity increased. In contrast to the linear increase in fluorescence intensity measured in the PTFE-filtered NCs, the fluorescence intensity of NCs filtered through nylon did not begin to increase significantly until after 10 minutes of NC growth, and then increased sigmoidally. The fluorescence line shape of NCs filtered through nylon did not include a peak at 600 nm, so the increase in fluorescence intensity measured at this wavelength was instead a result of the broad feature centered at 650 nm. The rate of increase in fluorescence intensity at 650 nm and 665 nm was similar to that measured in PTFE-filtered NCs, with the fluorescence intensity at the redder wavelength increasing faster, again indicating that the fluorescence feature spanning this wavelength range was redshifting as it increased in intensity.

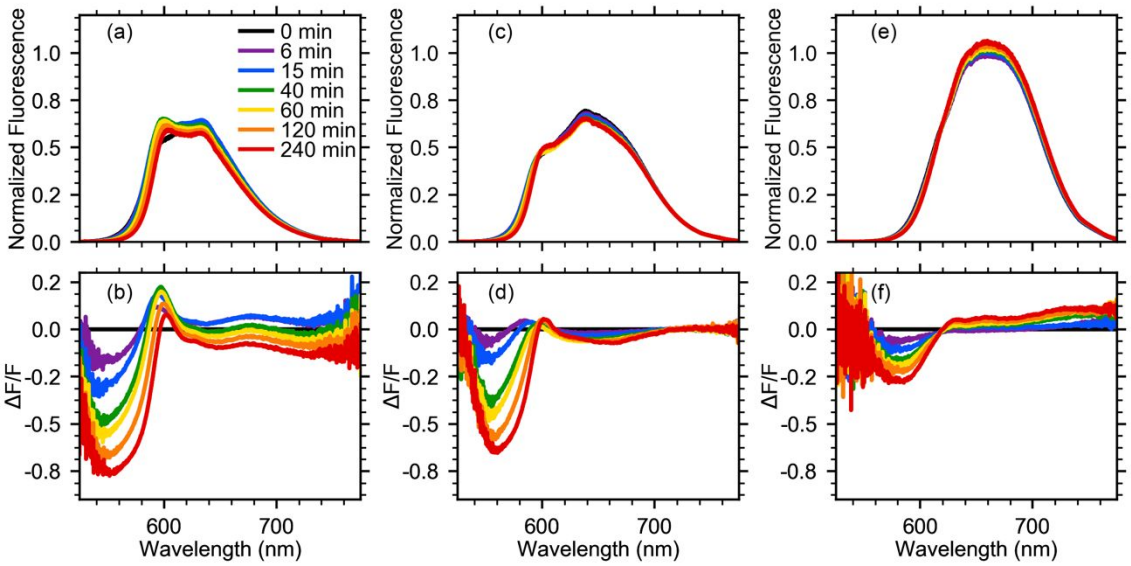

Figure 5: Aging of perovskite NCs grown for 15 (a,b), 35 (c,d), and 120 (e,f) minutes after filtering through PTFE, monitored by fluorescence (a,c,e) and normalized differential fluorescence (b,d,f). Fluorescence of filtered reaction mixture was re-measured at several ages post-filtration to observe how the NCs changed over time. Differential fluorescence spectra are the difference between the emission spectrum at each post-filtration time point and the spectrum recorded immediately following filtration, normalized by the intensity of the fluorescence spectrum immediately following filtration.

Nanocrystal Aging and Degradation

Analyzing the stability of the nascent NCs at different stages of growth provides deeper insight into the composition of these transient species. Aliquots of the reaction solution were extracted after 15, 35, and 120 minutes of growth and immediately filtered through a PTFE or nylon filter, Figure 5 and Figure S4, respectively. We measured the absorbance and fluorescence spectra of each solution at a series of time points after filtration, which we term the 'age' of the NCs post-filtration. Figure 5a,c,e shows the fluorescence of PTFE-filtered NC solutions as they aged. After 15 minutes of growth the emission spectrum measured immediately after filtration exhibited two peaks. Six minutes after filtration, the intensity of the blue edge of the fluorescence spectrum (<580 nm) had decreased. As the solution continued to age, the portion of the blue edge of the spectrum that decreased in intensity widened, up to 585 nm after 40 minutes and up to 590 nm after 120 minutes of aging. This is more clearly visualized by plotting the difference between the fluorescence spectra collected during aging and the spectrum measured immediately after filtration, Figure 5b. This plot indicates that the smallest NCs in the solution were the least stable and dissolved back into precursors. While the blue-edge of the spectrum receded, the red-edge of the fluorescence feature centered at 600 nm and the broader fluorescence peak at 635 nm grew. We ascribe these spectral changes to Ostwald ripening, whereby the precursor and ligand that are liberated when the smaller NCs dissolve are recruited into the larger NCs, enabling them to grow and become better passivated. However, all of these features eventually receded as the NCs continued to age, indicating that after only 15 minutes of growth even the largest NCs in the reaction mixture were unstable. In addition to the higher solubility of small NCs, these nascent NCs are likely also poorly-capped by organic ligands, as suggested by the lack of detectable emission from these samples after filtration with a polar nylon filter, Figure 3.

There was markedly less change in the fluorescence spectrum during the aging of NCs grown for 35 minutes, Figure 5c,d compared to that of NCs isolated after only 15 minutes of growth, indicating that the more mature NCs exhibited increased stability. The primary fluorescence peak was slightly redshifted to 638 nm owing to the longer growth time. The fluorescence spectrum was more stable and did not lose as much intensity over the 240 minutes of aging. The shoulder on the high-energy side of the spectrum redshifted as the NCs aged and underwent Ostwald ripening. However, unlike the spectrum in Figure 5a, the intensity of this fluorescence peak did not decrease. The spectral changes during aging of the NCs following 35 minutes of growth were smaller than those during the aging of the NCs grown for only 15 minutes, since fewer unstable small and poorly-capped NCs remained after the increased growth time. The increased stability of NCs that have grown to be larger and better capped is supported by the observation of emission in the nylon-filtered reaction solution after 35 minutes of growth.

NCs that have grown for 120 minutes, the full length of our experiment, are significantly more stable than earlier NC samples, Figure 5e,f. Over the first two hours of aging the spectrum lost intensity on the high energy shoulder and the primary peak continued to grow in intensity and redshift slightly, which we again ascribe to Ostwald ripening. During the four hours of aging the NC fluorescence continued to gain intensity, which we interpret as continued improvement in NC passivation by organic capping ligands. Comparing the magnitude of the fluorescence changes during aging in Figure 5b,d,f, clearly indicates that the NCs continued to become more stable during growth.

Two stages of NC formation, each with a distinct rate of increase in fluorescence intensity, are shown in Figure 3a. The measurements during the aging of the sample extracted after 15 minutes of growth indicate that NCs were unstable during the first stage of growth, Figure 5a,b. After proceeding to the second stage of formation, the NCs were more stable, as demonstrated in the fluorescence spectra measured during the aging of NCs after 35 and 120 minutes of growth, Figure 5c-f. This suggests that the structural changes during the second stage of formation, after 20 minutes in the case of this particular reaction, result in a dramatic improvement in stability. This could be owing to the NCs exceeding a size threshold beyond which they were insoluble, or that the surface ligation of the NCs was increasing. The rapid increase in fluorescence intensity measured in samples that can pass a polar nylon filter during the second formation stage suggests a change in the polarity of the NC surface. Thus, surface ligation is likely occurring during the second stage of NC formation. This may also be accompanied by continued NC growth, as suggested by the continuing redshift of the primary fluorescence feature. TEM characterization in Figure 2 supports this final ligation process, as there is no difference in the average size of the NCs that pass through either PTFE or nylon filters. Thus, any difference in the fluorescence must be owing to changes in surface passivation.

The distinct change in the rate of fluorescence intensity increase after 20 minutes of growth in the PTFE-filtered NCs and the simultaneous appearance of detectable fluorescence intensity in the nylon-filtered samples suggests that the beginning of the surface ligation stage was a distinct point in the reaction at which some threshold was crossed. It is possible that the free energy of the NC surface depends on its curvature, changing the equilibrium between bound and unbound ligands as the NCs grow. Further experiments will be needed to validate this hypothesis.

Dilution Studies of NC Aggregation

As illustrated in Figure 1c, one possible mechanism for NC formation is aggregative growth. In this mechanism small, poorly-capped NCs nucleate to form NC aggregates, and these aggregates then undergo rearrangement to fuse into one larger NC. To determine if the second stage of NC formation we have observed in our reaction is aggregative nucleation and growth we diluted NC samples filtered at various stages of growth. If aggregative nucleation occurred at 20 minutes, initiating the second growth stage, dilution of a sample filtered after 20

minutes of growth would cause these newly formed aggregates to break apart into the smaller precursor NCs that existed at the end of the first stage of formation. The fluorescence spectrum of the PTFE-filtered sample grown for 20 minutes did change upon dilution, Figure S5a. The intensity ratio of the shoulder at 600 nm to the main peak increased, indicating a shift back to the NC species dominant at shorter reaction times. This was not observed in the PTFE-filtered samples grown for 35 minutes, suggesting increased stability, Figure S5b. This could either indicate that the measured species after 20 minutes of growth were NC aggregates that were broken apart by dilution, or that the NCs were poorly-capped, unstable, and susceptible to Ostwald ripening, particularly after dilution changed the ratio of bound:unbound ligand to remove even more ligands from the NC surfaces.

If the distinct growth stage observed 20 minutes into the reaction was indeed aggregative nucleation, an aliquot filtered through nylon at that time would consist of newly formed aggregates with capped surfaces. Dilution of this sample should then exhibit the fluorescence features of NCs during the first stage of formation after filtration through PTFE, since the newly exposed NC surfaces would be poorly-capped. The emission spectra in Figure S5c exhibited neither a blueshift nor the reappearance of the 600 nm peak. This indicates that aggregative nucleation was not responsible for the observed second stage of NC formation.

A previous fluorescence study of formamidinium lead halide NCs showed that NCs during the early stages of growth exhibit sharp, high energy fluorescence peaks attributed to formation of nanoplatelets (NPTs) as intermediates.[67] These spectral features are very similar in nature to the fluorescence we observed during our reactions. It is possible that the species we observed during the first stage of NC formation are poorly-capped NPTs that can be adsorbed to nylon filters. If NCs were formed by the aggregation of these NPTs, we would expect dilution to break the aggregates back into NPTs, which was not observed.

Conclusions

Our results demonstrate that sub-populations of NCs can be selected based on their surface properties through choice of filter material. Applying this to a solvation-mediated synthesis has enabled spectroscopic investigation of nucleation and growth during a perovskite NC synthesis. The data suggest that in this type of reaction NCs exhibit classical, non-aggregative growth, potentially via a series of NPT intermediates, with a final surface ligation phase where poorly-capped NCs become well-passivated by surface ligands. TEM images that show NC populations with identical size and morphology distributions but different fluorescence intensities lend further evidence to the existence of this final ligation stage. The presented approach to sampling a reaction mixture during a NC synthesis opens the door for the application of time-resolved spectroscopies to the study of perovskite NCs during synthesis, which will provide further insight into the mechanism by which these NCs form. Future work will involve examining how NC electronic structure is affected by changing reaction conditions during different stages of NC formation, providing a deeper understanding of the emergence of NC photophysics.

Conflicts of interest

There are no conflicts to declare.

Acknowledgements

This material is based upon work supported by the National Science Foundation REU under Grant No. CHE-1659346. M.L.C. acknowledges financial support from ARCS Oregon Chapter. Josh Razink is acknowledged for assistance with TEM measurements and useful discussions during analysis.

References

1 L. C. Schmidt, A. Pertegás, S. González-Carrero, O. Malinkiewicz, S. Agouram, G. Mínguez Espallargas, H. J. Bolink, R. E. Galian and J. Pérez-Prieto, Nontemplate Synthesis of CH3NH3PbBr3 Perovskite Nanoparticles, *J. Am. Chem. Soc.*, 2014, **136**, 850–853.

2 G. Li, F. W. R. Rivarola, N. J. L. K. Davis, S. Bai, T. C. Jellicoe, F. de la Peña, S. Hou, C. Ducati, F. Gao, R. H. Friend, N. C. Greenham and Z.-K. Tan, Highly Efficient Perovskite Nanocrystal Light-Emitting Diodes Enabled by a Universal Crosslinking Method, *Adv. Mater.*, 2016, **28**, 3528–3534.

3 S. Yakunin, L. Protesescu, F. Krieg, M. I. Bodnarchuk, G. Nedelcu, M. Humer, G. D. Luca, M. Fiebig, W. Heiss and M. V. Kovalenko, Low-threshold amplified spontaneous emission and lasing from colloidal nanocrystals of caesium lead halide perovskites, *Nat. Commun.*, 2015, **6**, 1–9.

4 B. Tang, H. Dong, L. Sun, W. Zheng, Q. Wang, F. Sun, X. Jiang, A. Pan and L. Zhang, Single-Mode Lasers Based on Cesium Lead Halide Perovskite Submicron Spheres, *ACS Nano*, 2017, **11**, 10681–10688.

5 G. Rainò, M. A. Becker, M. I. Bodnarchuk, R. F. Mahrt, M. V. Kovalenko and T. Stöferle, Superfluorescence from lead halide perovskite quantum dot superlattices, *Nature*, 2018, **563**, 671–675.

6 Y. Dong, Y. Zhao, S. Zhang, Y. Dai, L. Liu, Y. Li and Q. Chen, Recent advances toward practical use of halide perovskite nanocrystals, *J. Mater. Chem. A*, 2018, **6**, 21729–21746.

7 Y. Hassan, Y. Song, R. D. Pensack, A. I. Abdelrahman, Y. Kobayashi, M. A. Winnik and G. D. Scholes, Structure-Tuned Lead Halide Perovskite Nanocrystals, *Adv. Mater.*, 2016, **28**, 566–573.

8 A. Pan, B. He, X. Fan, Z. Liu, J. J. Urban, A. P. Alivisatos, L. He and Y. Liu, Insight into the Ligand-Mediated Synthesis of Colloidal CsPbBr3 Perovskite Nanocrystals: The Role of Organic Acid, Base, and Cesium Precursors, *ACS Nano*, 2016, **10**, 7943–7954.

9 J. Shamsi, Z. Dang, P. Bianchini, C. Canale, F. Di Stasio, R. Brescia, M. Prato and L. Manna, Colloidal Synthesis of Quantum Confined Single Crystal CsPbBr3 Nanosheets with Lateral Size Control up to the Micrometer Range, *J. Am. Chem. Soc.*, 2016, **138**, 7240–7243.

10 A. De, N. Mondal and A. Samanta, Luminescence tuning and exciton dynamics of Mn-doped CsPbCl 3 nanocrystals, *Nanoscale*, 2017, **9**, 16722–16727.

11 F. Zhang, C. Chen, S. V. Kershaw, C. Xiao, J. Han, B. Zou, X. Wu, S. Chang, Y. Dong, A. L. Rogach and H. Zhong, Ligand-Controlled Formation and Photoluminescence Properties of CH3NH3PbBr3 Nanocubes and Nanowires, *ChemNanoMat*, 2017, **3**, 303–310.

12 M. B. Teunis, M. A. Johnson, B. B. Muhoberac, S. Seifert and R. Sardar, Programmable Colloidal Approach to Hierarchical Structures of Methylammonium Lead Bromide Perovskite Nanocrystals with Bright Photoluminescent Properties, *Chem. Mater.*, 2017, **29**, 3526–3537.
13 A. Dutta, S. K. Dutta, S. Das Adhikari and N. Pradhan, Tuning the Size of CsPbBr3 Nanocrystals: All at One Constant Temperature, *ACS Energy Lett.*, 2018, **3**, 329–334.
14 L. Peng, A. Dutta, R. Xie, W. Yang and N. Pradhan, Dot–Wire–Platelet–Cube: Step Growth and Structural Transformations in CsPbBr3 Perovskite Nanocrystals, *ACS Energy Lett.*, 2018, **3**, 2014–2020.
15 V. K. LaMer and R. H. Dinegar, Theory, Production and Mechanism of Formation of Monodispersed Hydrosols, *J. Am. Chem. Soc.*, 1950, **72**, 4847–4854.
16 Y. Yin and A. P. Alivisatos, Colloidal nanocrystal synthesis and the organic–inorganic interface, *Nature*, 2005, **437**, 664–670.
17 T. Sugimoto, Underlying mechanisms in size control of uniform nanoparticles, *J. Colloid Interface Sci.*, 2007, **309**, 106–118.
18 N. T. K. Thanh, N. Maclean and S. Mahiddine, Mechanisms of Nucleation and Growth of Nanoparticles in Solution, *Chem. Rev.*, 2014, **114**, 7610–7630.
19 L. Protesescu, S. Yakunin, M. I. Bodnarchuk, F. Krieg, R. Caputo, C. H. Hendon, R. X. Yang, A. Walsh and M. V. Kovalenko, Nanocrystals of Cesium Lead Halide Perovskites (CsPbX3, X = Cl, Br, and I): Novel Optoelectronic Materials Showing Bright Emission with Wide Color Gamut, *Nano Lett.*, 2015, **15**, 3692–3696.
20 C. B. Murray, D. J. Norris and M. G. Bawendi, Synthesis and characterization of nearly monodisperse CdE (E = sulfur, selenium, tellurium) semiconductor nanocrystallites, *J. Am. Chem. Soc.*, 1993, **115**, 8706–8715.
21 Y.-H. Lu, W.-H. Lin, C.-Y. Yang, Y.-H. Chiu, Y.-C. Pu, M.-H. Lee, Y.-C. Tseng and Y.-J. Hsu, A facile green antisolvent approach to Cu 2+ -doped ZnO nanocrystals with visible-light-responsive photoactivities, *Nanoscale*, 2014, **6**, 8796–8803.
22 Q. A. Akkerman, S. G. Motti, A. R. Srimath Kandada, E. Mosconi, V. D'Innocenzo, G. Bertoni, S. Marras, B. A. Kamino, L. Miranda, F. De Angelis, A. Petrozza, M. Prato and L. Manna, Solution Synthesis Approach to Colloidal Cesium Lead Halide Perovskite Nanoplatelets with Monolayer-Level Thickness Control, *J. Am. Chem. Soc.*, 2016, **138**, 1010–1016.
23 S. Seth and A. Samanta, A Facile Methodology for Engineering the Morphology of $CsPbX_3$ Perovskite Nanocrystals under Ambient Condition, *Sci. Rep.*, 2016, **6**, 37693.
24 Y. Pu, F. Cai, D. Wang, J.-X. Wang and J.-F. Chen, Colloidal Synthesis of Semiconductor Quantum Dots toward Large-Scale Production: A Review, *Ind. Eng. Chem. Res.*, 2018, **57**, 1790–1802.
25 Y. Tong, E. Bladt, M. F. Aygüler, A. Manzi, K. Z. Milowska, V. A. Hintermayr, P. Docampo, S. Bals, A. S. Urban, L. Polavarapu and J. Feldmann, Highly Luminescent Cesium Lead Halide Perovskite Nanocrystals with Tunable Composition and Thickness by Ultrasonication, *Angew. Chem. Int. Ed.*, 2016, **55**, 13887–13892.
26 Y. Li, H. Huang, Y. Xiong, S. V. Kershaw and A. L. Rogach, Revealing the Formation Mechanism of CsPbBr3 Perovskite Nanocrystals Produced via a Slowed-Down Microwave-Assisted Synthesis, *Angew. Chem. Int. Ed.*, 2018, **57**, 5833–5837.
27 K. G. Stamplecoskie, J. S. Manser and P. V. Kamat, Dual nature of the excited state in organic–inorganic lead halide perovskites, *Energy Environ. Sci.*, 2014, **8**, 208–215.
28 F. Li, L. Cao, S. Shi, H. Gao, L. Song, C. Geng, W. Bi and S. Xu, Controlled Growth of CH3NH3PbBr3 Perovskite Nanocrystals via a Water–Oil Interfacial Synthesis Method, *Angew. Chem. Int. Ed.*, , DOI:10.1002/anie.201910225.
29 W. Ostwald, Über die vermeintliche Isomerie des roten und gelben Quecksilberoxyds und die Oberflächenspannung fester Körper, *Z. Für Phys. Chem.*, 1900, **34U**, 495–503.
30 I. M. Lifshitz and V. V. Slyozov, The kinetics of precipitation from supersaturated solid solutions, *J. Phys. Chem. Solids*, 1961, **19**, 35–50.
31 C. Wagner, Theorie der Alterung von Niederschlägen durch Umlösen (Ostwald-Reifung), *Z. Für Elektrochem. Berichte Bunsenges. Für Phys. Chem.*, 1961, **65**, 581–591.
32 P. W. Voorhees, The theory of Ostwald ripening, *J. Stat. Phys.*, 1985, **38**, 231–252.
33 N. Pradhan, D. Reifsnyder, R. Xie, J. Aldana and X. Peng, Surface Ligand Dynamics in Growth of Nanocrystals, *J. Am. Chem. Soc.*, 2007, **129**, 9500–9509.
34 Y. Xia, Y. Xiong, B. Lim and S. E. Skrabalak, Shape-Controlled Synthesis of Metal Nanocrystals: Simple Chemistry Meets Complex Physics?, *Angew. Chem. Int. Ed.*, 2009, **48**, 60–103.
35 C. R. Bealing, W. J. Baumgardner, J. J. Choi, T. Hanrath and R. G. Hennig, Predicting Nanocrystal Shape through Consideration of Surface-Ligand Interactions, *ACS Nano*, 2012, **6**, 2118–2127.
36 X. Xia, S. Xie, M. Liu, H.-C. Peng, N. Lu, J. Wang, M. J. Kim and Y. Xia, On the role of surface diffusion in determining the shape or morphology of noble-metal nanocrystals, *Proc. Natl. Acad. Sci.*, 2013, **110**, 6669–6673.
37 D. Yang, X. Li and H. Zeng, Surface Chemistry of All Inorganic Halide Perovskite Nanocrystals: Passivation Mechanism and Stability, *Adv. Mater. Interfaces*, 2018, **5**, 1701662.
38 M. D. Peterson, L. C. Cass, R. D. Harris, K. Edme, K. Sung and E. A. Weiss, The Role of Ligands in Determining the Exciton Relaxation Dynamics in Semiconductor Quantum Dots, *Annu. Rev. Phys. Chem.*, 2014, **65**, 317–339.
39 M. A. Boles, D. Ling, T. Hyeon and D. V. Talapin, The surface science of nanocrystals, *Nat. Mater.*, 2016, **15**, 141.
40 M. B. Teunis, T. Liyanage, S. Dolai, B. B. Muhoberac, R. Sardar and M. Agarwal, Unraveling the Mechanism Underlying Surface Ligand Passivation of Colloidal Semiconductor Nanocrystals: A Route for Preparing Advanced Hybrid Nanomaterials, *Chem. Mater.*, 2017, **29**, 8838–8849.
41 F. Wang, V. N. Richards, S. P. Shields and W. E. Buhro, Kinetics and Mechanisms of Aggregative Nanocrystal Growth, *Chem. Mater.*, 2014, **26**, 5–21.
42 J. S. Steckel, B. K. H. Yen, D. C. Oertel and M. G. Bawendi, On the Mechanism of Lead Chalcogenide Nanocrystal Formation, *J. Am. Chem. Soc.*, 2006, **128**, 13032–13033.
43 H. Liu, J. S. Owen and A. P. Alivisatos, Mechanistic Study of Precursor Evolution in Colloidal Group II–VI Semiconductor Nanocrystal Synthesis, *J. Am. Chem. Soc.*, 2007, **129**, 305–312.
44 K. Yu, M. Z. Hu, R. Wang, M. L. Piolet, M. Frotey, Md. B. Zaman, X. Wu, D. M. Leek, Y. Tao, D. Wilkinson and C. Li, Thermodynamic Equilibrium-Driven Formation of Single-Sized Nanocrystals: Reaction Media Tuning CdSe Magic-Sized versus Regular Quantum Dots, *J. Phys. Chem. C*, 2010, **114**, 3329–3339.
45 J. S. Owen, E. M. Chan, H. Liu and A. P. Alivisatos, Precursor Conversion Kinetics and the Nucleation of Cadmium Selenide Nanocrystals, *J. Am. Chem. Soc.*, 2010, **132**, 18206–18213.
46 K. Yu, CdSe Magic-Sized Nuclei, Magic-Sized Nanoclusters and Regular Nanocrystals: Monomer Effects on Nucleation and Growth, *Adv. Mater.*, 2012, **24**, 1123–1132.
47 K. De Nolf, R. K. Capek, S. Abe, M. Sluydts, Y. Jang, J. C. Martins, S. Cottenier, E. Lifshitz and Z. Hens, Controlling the Size of Hot Injection Made Nanocrystals by Manipulating the Diffusion Coefficient of the Solute, *J. Am. Chem. Soc.*, 2015, **137**, 2495–2505.
48 J. Li, H. Wang, L. Lin, Q. Fang and X. Peng, Quantitative Identification of Basic Growth Channels for Formation of Monodisperse Nanocrystals, *J. Am. Chem. Soc.*, 2018, **140**, 5474–5484.
49 J. Turkevich, P. C. Stevenson and J. Hillier, A study of the nucleation and growth processes in the synthesis of colloidal gold, *Discuss. Faraday Soc.*, 1951, **11**, 55–75.

50 T. Sugimoto, F. Shiba, T. Sekiguchi and H. Itoh, Spontaneous nucleation of monodisperse silver halide particles from homogeneous gelatin solution I: silver chloride, *Colloids Surf. Physicochem. Eng. Asp.*, 2000, **164**, 183–203.
51 T. Sugimoto and F. Shiba, Spontaneous nucleation of monodisperse silver halide particles from homogeneous gelatin solution II: silver bromide, *Colloids Surf. Physicochem. Eng. Asp.*, 2000, **164**, 205–215.
52 J. Wang, H. F. M. Boelens, M. B. Thathagar and G. Rothenberg, In Situ Spectroscopic Analysis of Nanocluster Formation, *ChemPhysChem*, 2004, **5**, 93–98.
53 D. Li, M. H. Nielsen, J. R. I. Lee, C. Frandsen, J. F. Banfield and J. J. D. Yoreo, Direction-Specific Interactions Control Crystal Growth by Oriented Attachment, *Science*, 2012, **336**, 1014–1018.
54 G. Kalyuzhny and R. W. Murray, Ligand Effects on Optical Properties of CdSe Nanocrystals, *J. Phys. Chem. B*, 2005, **109**, 7012–7021.
55 B. Luo, Y.-C. Pu, S. A. Lindley, Y. Yang, L. Lu, Y. Li, X. Li and J. Z. Zhang, Organolead Halide Perovskite Nanocrystals: Branched Capping Ligands Control Crystal Size and Stability, *Angew. Chem. Int. Ed.*, 2016, **55**, 8864–8868.
56 X. Zheng, Y. Hou, H.-T. Sun, O. F. Mohammed, E. H. Sargent and O. M. Bakr, Reducing Defects in Halide Perovskite Nanocrystals for Light-Emitting Applications, *J. Phys. Chem. Lett.*, 2019, **10**, 2629–2640.
57 H. Huang, Q. Xue, B. Chen, Y. Xiong, J. Schneider, C. Zhi, H. Zhong and A. L. Rogach, Top-Down Fabrication of Stable Methylammonium Lead Halide Perovskite Nanocrystals by Employing a Mixture of Ligands as Coordinating Solvents, *Angew. Chem. Int. Ed.*, 2017, **56**, 9571–9576.
58 L. Wang, N. E. Williams, E. W. Malachosky, J. P. Otto, D. Hayes, R. E. Wood, P. Guyot-Sionnest and G. S. Engel, Scalable Ligand-Mediated Transport Synthesis of Organic–Inorganic Hybrid Perovskite Nanocrystals with Resolved Electronic Structure and Ultrafast Dynamics, *ACS Nano*, 2017, **11**, 2689–2696.
59 Y. Hassan, O. J. Ashton, J. H. Park, G. Li, N. Sakai, B. Wenger, A.-A. Haghighirad, N. K. Noel, M. H. Song, B. R. Lee, R. H. Friend and H. J. Snaith, Facile Synthesis of Stable and Highly Luminescent Methylammonium Lead Halide Nanocrystals for Efficient Light Emitting Devices, *J. Am. Chem. Soc.*, 2019, **141**, 1269–1279.
60 L. Qu, W. W. Yu and X. Peng, In Situ Observation of the Nucleation and Growth of CdSe Nanocrystals, *Nano Lett.*, 2004, **4**, 465–469.
61 Y. Tong, F. Ehrat, W. Vanderlinden, C. Cardenas-Daw, J. K. Stolarczyk, L. Polavarapu and A. S. Urban, Dilution-Induced Formation of Hybrid Perovskite Nanoplatelets, *ACS Nano*, 2016, **10**, 10936–10944.
62 Z. Dang, J. Shamsi, F. Palazon, M. Imran, Q. A. Akkerman, S. Park, G. Bertoni, M. Prato, R. Brescia and L. Manna, In Situ Transmission Electron Microscopy Study of Electron Beam-Induced Transformations in Colloidal Cesium Lead Halide Perovskite Nanocrystals, *ACS Nano*, 2017, **11**, 2124–2132.
63 N. Klein-Kedem, D. Cahen and G. Hodes, Effects of Light and Electron Beam Irradiation on Halide Perovskites and Their Solar Cells, *Acc. Chem. Res.*, 2016, **49**, 347–354.
64 Z. Dang, J. Shamsi, Q. A. Akkerman, M. Imran, G. Bertoni, R. Brescia and L. Manna, Low-Temperature Electron Beam-Induced Transformations of Cesium Lead Halide Perovskite Nanocrystals, *ACS Omega*, 2017, **2**, 5660–5665.
65 I. Lignos, S. Stavrakis, G. Nedelcu, L. Protesescu, A. J. deMello and M. V. Kovalenko, Synthesis of Cesium Lead Halide Perovskite Nanocrystals in a Droplet-Based Microfluidic Platform: Fast Parametric Space Mapping, *Nano Lett.*, 2016, **16**, 1869–1877.
66 I. Lignos, R. Maceiczyk and A. J. deMello, Microfluidic Technology: Uncovering the Mechanisms of Nanocrystal Nucleation and Growth, *Acc. Chem. Res.*, 2017, **50**, 1248–1257.
67 R. M. Maceiczyk, K. Dümbgen, I. Lignos, L. Protesescu, M. V. Kovalenko and A. J. deMello, Microfluidic Reactors Provide Preparative and Mechanistic Insights into the Synthesis of Formamidinium Lead Halide Perovskite Nanocrystals, *Chem. Mater.*, 2017, **29**, 8433–8439.
68 H. Reiss, The Growth of Uniform Colloidal Dispersions, *J. Chem. Phys.*, 1951, **19**, 482–487.
69 D. B. K. Chu, J. S. Owen and B. Peters, Nucleation and Growth Kinetics from LaMer Burst Data, *J. Phys. Chem. A*, 2017, **121**, 7511–7517.
70 J. C. Sadighian, M. L. Crawford and C. Y. Wong, Rapid sampling during synthesis of lead halide perovskite nanocrystals for spectroscopic measurement, *MRS Adv.*, 2019, **4**, 1957–1964.
71 T. Chiba, K. Hoshi, Y.-J. Pu, Y. Takeda, Y. Hayashi, S. Ohisa, S. Kawata and J. Kido, High-Efficiency Perovskite Quantum-Dot Light-Emitting Devices by Effective Washing Process and Interfacial Energy Level Alignment, *ACS Appl. Mater. Interfaces*, 2017, **9**, 18054–18060.
72 C. Xiao, Z. Li, H. Guthrey, J. Moseley, Y. Yang, S. Wozny, H. Moutinho, B. To, J. J. Berry, B. Gorman, Y. Yan, K. Zhu and M. Al-Jassim, Mechanisms of Electron-Beam-Induced Damage in Perovskite Thin Films Revealed by Cathodoluminescence Spectroscopy, *J. Phys. Chem. C*, 2015, **119**, 26904–26911.
73 A. R. Milosavljević, W. Huang, S. Sadhu and S. Ptasinska, Low-Energy Electron-Induced Transformations in Organolead Halide Perovskite, *Angew. Chem. Int. Ed.*, 2016, **55**, 10083–10087.
74 B. Philippe, B.-W. Park, R. Lindblad, J. Oscarsson, S. Ahmadi, E. M. J. Johansson and H. Rensmo, Chemical and Electronic Structure Characterization of Lead Halide Perovskites and Stability Behavior under Different Exposures—A Photoelectron Spectroscopy Investigation, *Chem. Mater.*, 2015, **27**, 1720–1731.
75 H. Yuan, E. Debroye, K. Janssen, H. Naiki, C. Steuwe, G. Lu, M. Moris, E. Orgiu, H. Uji-i, F. De Schryver, P. Samorì, J. Hofkens and M. Roeffaers, Degradation of Methylammonium Lead Iodide Perovskite Structures through Light and Electron Beam Driven Ion Migration, *J. Phys. Chem. Lett.*, 2016, **7**, 561–566.